Radiation Effects and Defects in Solids, Vol. 142, pp. 205–221
Reprints available directly from the publisher
Photocopying permitted by license only

COMPUTER SIMULATION OF PARTICLE BOMBARDMENT OF ALKANETHIOL CHAINS ADSORBED ON GOLD SURFACE

K.S.S. LIU[a,*], J.C. VICKERMAN[a] and B.J. GARRISON[b]

[a] *Surface Analysis Research Centre, Department of Chemistry, UMIST, PO Box 88, Manchester, M60 1QD, UK;* [b] *Department of Chemistry, The Pennsylvania State University, University Park, PA 16802, USA*

(Received 22 July 1996; Revised 12 September 1996)

Molecular dynamics (MD) simulations have been used to model the high energy particle bombardment process of deuterated alkanethiol chains chemisorbed on a gold surface. The model involves the use of sophisticated many-body potential energy functions to represent the chemical interactions among atoms. We have investigated the dependence of the fragmentation pattern upon two different angles of the Ar incidents, namely in the direction parallel (−35°) and orthogonal (+55°) to the tilt chain. It is found that surface thiol chains are likely to be hit for Ar at +55° so that more fragmentation occurs. In contrast, collisions with substrate atoms are more likely when Ar impacts at −35°. This leads to less fragmentation and more molecular species are sputtered. We also found that hydrocarbon fragments such as C_2D_5, C_3D_7, and C_4D_9 are prominent for both angles of incidence although the suggested mechanisms leading to their ejections are different.

Keywords: Molecular dynamics; Bombardment; Alkanethiol; Self-assembled monolayer

INTRODUCTION

The high energy particle bombardment process has been shown to be a powerful method for probing features characteristic of a surface [1]. It involves the use of a high-energy primary beam which is directed onto the system of interest and results in the ejection of atomic or molecular ions for subsequent analysis. The energy of the impinging particle,

* Corresponding author.

usually between 500 – 25,000 eV, is well beyond that of a typical chemical bond (2 – 7 eV). As the primary particle collides with the solid, a portion of its energy is transferred into it, causing both atomic and molecular species to eject into the vacuum. These ejected species can then be detected by spectrometers such as quadrupoles or time-of-flight systems [1], to extract information including their identity, energy and angle of ejection.

One of the important applications of this process lies in its ability to observe intermediates involved in complex catalytic reactions [2–4]. The mass spectral data of the ejected species can be used to identify molecular species. Fingerprint regions have been established for a variety of complex materials. It is, however, often unclear what leads to a given fingerprint and the underlying mechanism for the ejected species. Sometimes, the molecular adsorbate or its catonised or protonated form is the largest peak in the mass spectra which makes interpretation of the mass spectra elementary. At other times, however, the largest peak may be a product of the unimolecular dissociation of the molecular adsorbate or the reaction of two or more adsorbates. The interpretation of the data in this case is not as simple. For this reason, information as to the mechanisms of ejection should help in the interpretation of the spectral data in terms of the identity of the original surface species. To this end, molecular dynamics (MD) computer simulations offer a powerful approach for following and understanding the atomic processes in the particle bombardment leading to molecular desorption [5–9]. Not only do these simulations provide valuable information about the mechanism and reaction pathways by which these processes occur, they also allow experimental variables to be varied which change the atomic motions, and thus the overall outcome of the chemical processes.

Among the MD studies, Taylor *et al.* [10 - 12] have investigated the effects of the bombardment process on various hydrocarbons adsorbed on a Pt surface. Mechanisms as to how these adsorbates eject have been investigated. Lateral motions are observed for particles in the region right above the surface leading to collisions with the neighbouring adsorbates.

In this work, we extended this approach to model the effects of particle bombardment on alkanethiol chains adsorbed on a gold surface. Alkanethiols are known to be spontaneously chemisorbed and self-assembled onto a gold substrate to form a highly crystalline, ordered and densely packed monolayers [13–17]. The interest in these self-assembled monolayers (SAMs) stems from their ease of preparation, high quality and stability and potential applications as sensors and non-linear optical devices.

In this study, our primary focus is to investigate the dependence of the fragmentation pattern upon two different angles of the incident Ar atom, namely in the direction parallel and orthogonal to the tilt chain. It is found that when an incident atom is directed at an angle orthogonal to the tilt angle of the thiol chain, surface organic atoms are likely to be hit so that more fragmentation occurs. In contrast, collisions with substrate atoms are more likely when the incident atom is directed at an angle parellel to the tilt chain. This leads to less fragmentation and more molecular species are sputtered. It is our aim to provide a mechanistic view for these fragmentation behaviours. We also found that hydrocarbon fragments such as C_2D_5, C_3D_7, and C_4D_9 are prominent for both angles of incidence although mechanisms leading to their ejections are different.

METHOD

The 700 eV Ar bombardment of thiol chains of $S-(CD_2)_4-CD_3$ chemisorbed on the Au(111) surface is studied via molecular dynamics (MD) computer simulations. Deuterium instead of hydrogen atoms are used in our model. The increase of mass for these atoms enable us to use larger time steps in our integration schemes, thus reducing the computational times. The classical calculations are based on the Gear-predictor algorithm [18] to evaluate the forces among the atoms.

The size of the substrate is chosen to be (32×18) layers in the xz-plane with 12 layers along the y-direction. A total of 68 alkanethiol molecules are adsorbed on the Au surface which is made large enough to retain the effects of the collisional impact. The S occupies every 3-fold site of the Au(111) surface in a $(3^{1/2} \times 3^{1/2})R30°$ hexagonal arrangement [14,15,19] as shown in (Fig. 1). The Au–S–C bond angle is 180°. The rest of the hydrocarbon chain tilts at about 35° to the surface normal. No periodic boundaries were used in our system as the inclusion of them would be physically incorrect. Before the integration of

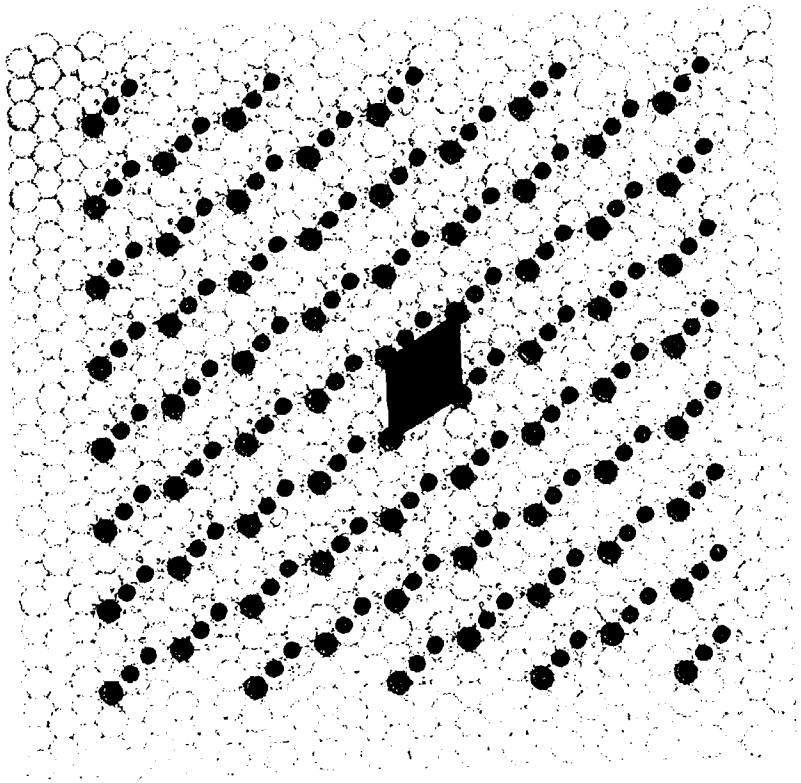

FIGURE 1 Hexagonal arrangement of S-$(CD_2)_4$-CD_3 alkanethiol chains occupying 3-folded sites of Au(111) surface. The impact zone is shown by a parallelogram. The white spheres represent Au atoms, the green sphere represent S atoms, the red spheres represent C atoms, and the light blue spheres represent H atoms. (See Color Plate IV.)

the equations of motion can begin, the initial conditions of the system are needed. The target atoms including both the substrate and adsorbate are specified with their initial positions in x-, y-, and z-coordinates. They all start with an initial velocity of 0 m/s which is achieved by quenching the system down to 0 K. Temperature effects are not taken into account in our study as it is believed that they are not the major factor that affect the sputtering process. Nevertheless, we are not at this stage to make detailed and quantitative comparisons with the experimental SIMS data, but rather in an attempt to explore possibilities that simulations can offer to this study. The kinetic energy of

700 eV for the incoming Ar atom was chosen and is found to be sufficient for our bombardment desorption study. While the azimuthal angle is kept constant at +45°, two polar angles have been chosen at −35° and +55° with respect to the surface normal. These angles direct the Ar atom in the direction which is parallel and orthogonal to the tilt chain respectively, as shown in Fig. 2. Experimentally one cannot aim the incoming beam at a specific atom on the surface. Thus, the experimental observables are taken as an average of all the possible aiming points. The space over which these aiming points (i.e. the impact zone) is dependent upon the system of study. As the thiol adsorbates are arranged in a hexagonal manner with a tilt angle of 35°, the impact zone is chosen to be a parallelogram as shown in (Fig. 1). The dynamics of the high energy bombardment process are over within 1–1.5 ps [12]. Beyond this time, energy for most of the atoms remaining in the solid are low such that ejection becomes insignificant. Therefore, each trajectory is allowed to run for 2 ps and a total of 100 trajectories have been run for each angle of incidence. At the end of each simulation, those atoms which have a velocity directed away from the surface and at a chosen height (5 Å above the adsorbate) are regarded as sputtered atoms. We have also introduced an imaginary boundary which lies 2 Å below the threshold level for ejection. This is needed to take care of those atoms which may still have interactions with other non-ejecting

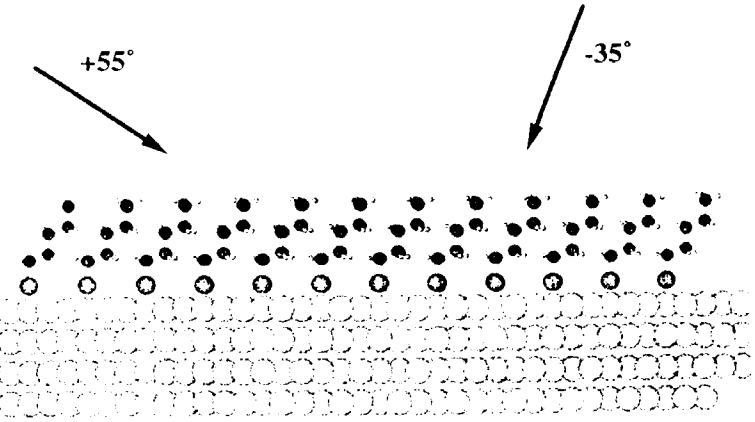

FIGURE 2 Side view of the initial configuration showing the approximate 35° tilt of the chains and the two polar angles of the Ar incidents. The atoms to which the coloured spheres represent are the same as those described in Fig. 1. (See Color Plate V.)

neighbouring atoms. If an isolated atom falls within this imaginary boundary and with a velocity directed away from the surface, we will consider this atom as sputtered. Finally, we also test for ejected clusters. The method is similar to that of testing for individual atom and is done by calculating the cluster–surface interaction energy. If the interaction energy is positive and with a velocity directed away from the surface, the cluster is considerd as sputtered.

The classical MD scheme has been described in detail elsewhere [6,7,20,21]. The forces among the various atoms are calculated using a well selected blend of empirical potential energy functions. The Ar–C, Ar–D, Ar–S and Ar–Au are described using a purely repulsive Moliere pair-wise potential energy function [22]. For the Au–Au interactions, we use a many-body potential function, namely the MD/MC-CEM [23,24] to calculate the interaction energy. The feature of this potential function is that it obeys reasonable coulombic behaviour at small internuclear separations which makes it particularly attractive for modelling high energy bombardment process. Rosencrance *et al.* [25] have used the function to study atomic desorption process from single crystal metals using keV ion bombardment and successfully reproduced features observed in experiments.

The C–C, C–D, D–D interactions are described with a reactive many-body potential function developed by Brenner [26,27]. The function has been used to describe the energetics of bulk diamond, graphite and a wide range of hydrocarbon molecules including radicals. Not only has this function been successfully applied in MD simulations of a variety of chemical reactions, it has also been recently used in simulations of high energy particle bombardment events [10–12]. In order to correctly describe the geometrical structure of the thiol chain, the S–C interactions, which are described with a Morse potential function [28], are blended into the Brenner hydrocarbon potential. This is achieved by treating the S atoms as if they were H atoms and assuming the S–C bonds are σ-like in character. In much the same way the Au–C interactions are described with a Lennard–Jones pair-wise potential [18] and blended into the Brenner potential function. A similar approach has also been adopted by Taylor *et al.* [12] in their hydrocarbon/Pt systems. The Au–D and S–D interactions are described with a Lennard–Jones pair-wise potential; and the Au–S and S–S interactions with a Morse potential. In the latter case, a Moliere function has been attached to the Morse repulsive wall to handle the highly repulsive collisions during the bombardment process. The binding energy for the alkanethiol chains to the Au surface is fitted to an experimental value of 44 kcal/mol [19].

RESULTS AND DISCUSSION

Calculated mass distributions are determined by counting the neutral species ejected within the 2 ps of the bombardment event. The neutral species are collected by a virtual detector with chosen configurations which allows the detection to be maximised. We do not take into account such experimental factors as ionisation probability, ion stability. Within the limit of the simulated time scale, possible further fragmentation of the larger clusters during the μs flight to the detector are not included. The calculated distributions are represented graphically as 'mass spectra' which provides a starting point for identifying dominant ejected species for further mechanistic analysis.

The results for 100 Ar impacts at −35° and +55° angles of incidence on the thiol/Au system are shown in Figs. 3 and 4 respectively. We have also analysed the results for 50 trajectories though they are not shown here. We found that the relative peak intensities in the two sets of results differ by less than 5%. We therefore, believe that any statistical uncertainties which may arise in the results are not large in this study. The peak intensities shown reflect the frequency of occurrence of particles being ejected. In the figures, only those ejected species of masses below 200 amu are presented. The intensity for each peak is the actual number of the ejected species counted. Peaks with intensity less than 10 are regarded as insignificant and are not shown in the figures. Some of the masses may consist of more than one kind of species and we have resolved them by including the number of each of these ejected species in brackets. Note that there are more fragmented species observed for the +55° case. The difference in the mass spectra for the two angles of incidence lies in the direction of their impact upon the thiol/Au system. For the −35° angle of incidence, the Ar atom collides with the Au substrate atoms. The desorption process is then initiated by momentum transfer from the substrate to the chains via the S atoms. This also results in more Au atoms being ejected, as evidenced in the

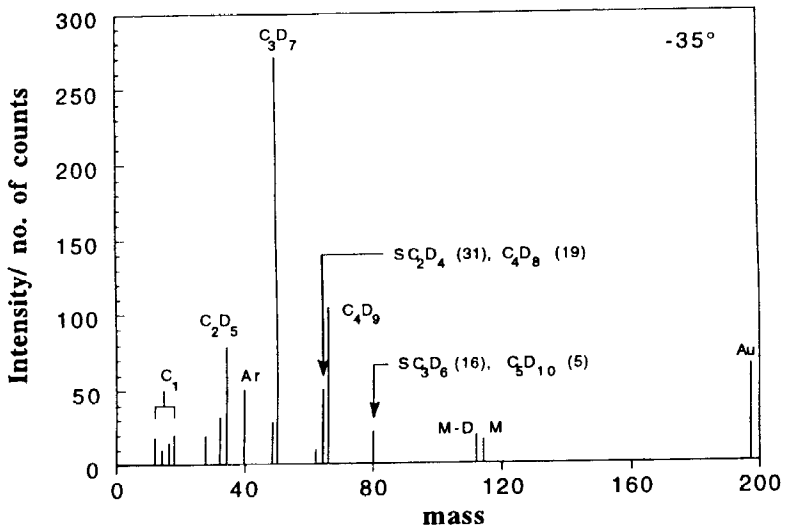

FIGURE 3 Mass spectra for Ar atom impact at −35° angle of incidence (parallel to the direction of the tilt angle of the chain).

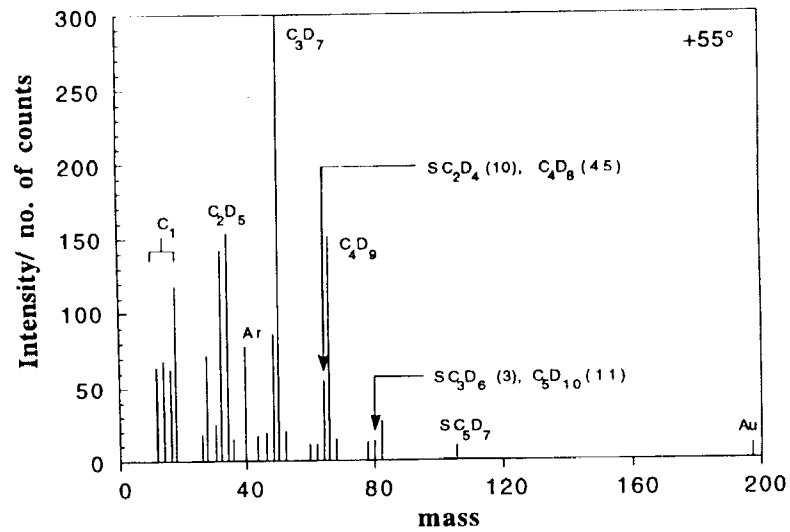

FIGURE 4 Mass spectra for Ar atom impact at +55° angle of incidence (orthogonal to the direction of the tilt angle of the chain).

mass spectra (cf. the Au peaks in Figs. 3 and 4). For the +55° impact, large amounts of Ar energy is transferred to the thiol atoms above the surface leading to more fragmentation along the chains.

While fundamental differences are recorded from the two impact angles, common features do exist in both cases. In particular, both show prominent peaks corresponding to hydrocarbon fragments of C_2D_5, C_3D_7, and C_4D_9. An analysis of these hydrocarbon fragments indicates that the majority of them originate from the top part of the chain. This agrees well with the observations reported by Taylor *et al.* [11]. The time distribution in Fig. 5 for the Ar impact at −35° shows the time of ejection in the order of $C_2D_5 < C_3D_7 < C_4D_9$. Since the C_3D_7 is by far the most abundant species that comes off, we have attempted to look at this fragment more closely to explain the trend observed in their times of ejection.

The $S-(CD_2)_4-CD_3$ has three bond axes perpendicular to the Au surface. If the C atom adjacent to the linker S is identified as C_1, then the first perpendicular axis runs through the $S-C_1$, bond, the second runs through the C_2-C_3 bond, and the third runs through the C_4-C_5 bond. Figs. 6(a)–(e) show the movie frames of the bombardment

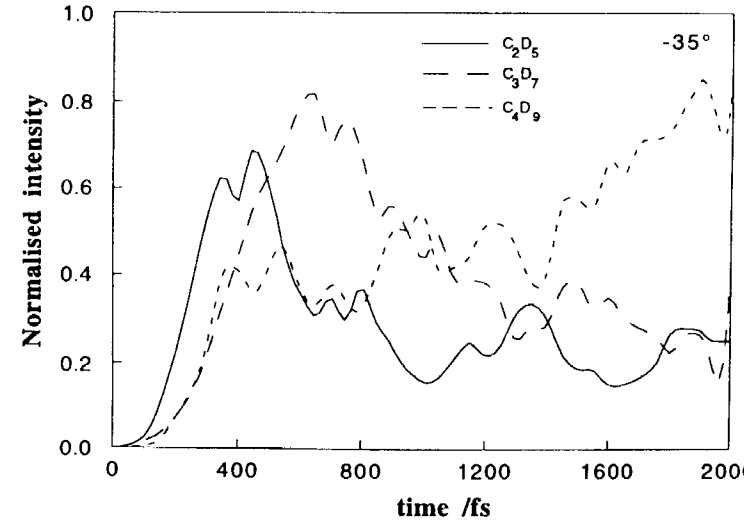

FIGURE 5 Time distribution for the ejection of the fragmented hydrocarbons with Ar at −35° to the surface normal.

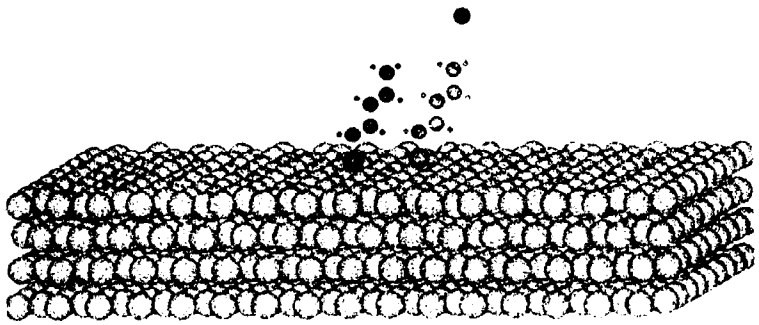

FIGURE 6(a)

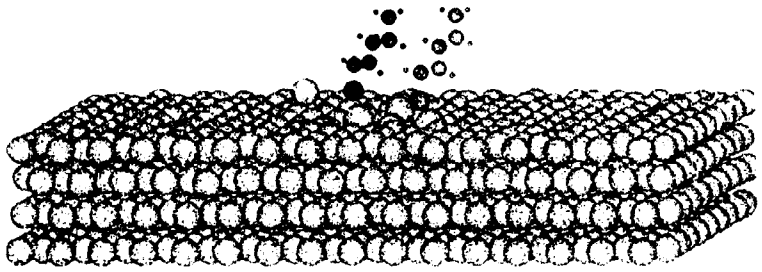

FIGURE 6(b)

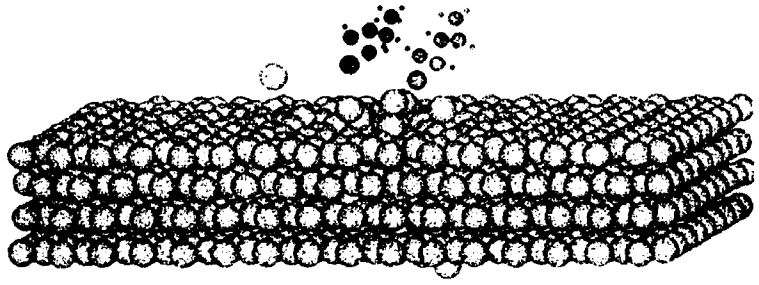

FIGURE 6(c)

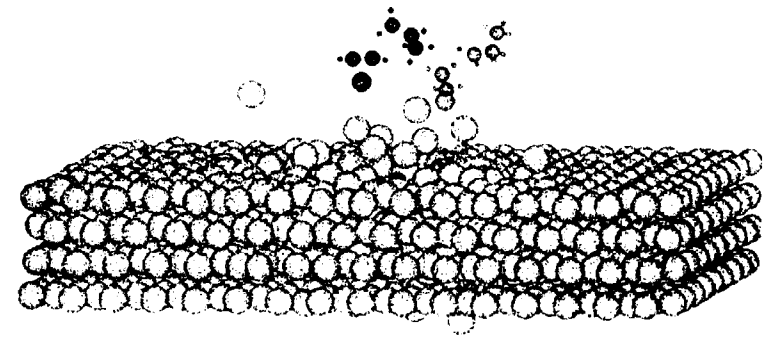

FIGURE 6(d)

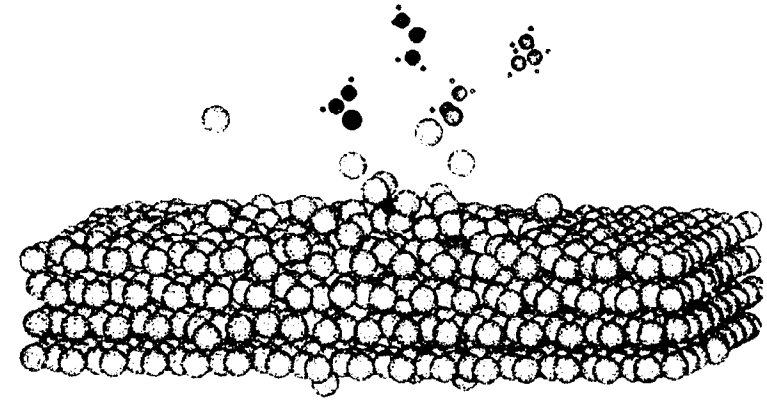

FIGURE 6(e)

FIGURE 6 Example of trajectory movie frames showing the formation of C_3D_7 hydrocarbon fragments. Only two chains relevant to the discussions are shown for clarity purpose. The light grey spheres represent Au atoms, and the red sphere represents Ar atom. The dark grey and green spheres represent the whole thiol chains including S, C and H atoms. (a) 0 fs. The Ar atom is at −35° to the surface normal. (b) 24 fs. Ar is embedded into the bulk. (c)–(d) 36–56 fs. Momentum transfer between the Au substrate and the adsorbates. The chain atoms recoil upwards. See text for detailed description of the events. (e) 82 fs. Subsequent to the recoil process results in the formation of C_3D_7 and SC_2D_4 fragments. (See Color Plates VI–X.)

process leading to the formation of C_3D_7 species. With the Ar bombardment at −35°, Fig. 6(a), the bulk obtains a large amount of momentum, Fig. 6(b). The atoms eventually recoil as they relax and bring the energy back to the surface. This process initiates motions across the surface Au atoms. As they move, they collide with the thiol adsorbates

and transfer their momentum through the S atoms, Fig. 6(c). This causes the $S-C_1$ bond to move upwards and in turn pulls the C_2-C_3 bond in the same direction. Provided that the momentum transfer is large and the motions near the bottom of the chain occur very fast, the C_3 atom recoils and pushes itself towards the C_4-C_5 bond, Fig. 6(d). The momentary formation of the $C_3-C_4-C_5$ ring and the continuous moving up of the C_3 atom subsequently lead to the scission of the C_2-C_3 bond. The process ends with the ejection of C_3H_7 with the C_3 pulling the C_4-C_5 atoms away from the surface, Fig. 6(e). We also observed peaks which correspond to $S-(CD_2)_2$ and $Au-S-(CD_2)_2$ suggesting that the energy gained by the lower portion of the chains is sufficiently large to detach themselves from the surface.

We find a similar ejection mechanism for the C_2D_5 fragments but the process occurs less frequently. Peaks such as $S-(CD_2)_3$ and their corresponding Au-clusters are also recorded though their intensity of ejection are low. The C_2D_5 fragments generally eject faster than the C_3D_7 fragments. This suggests that the momentum gained by the chain in this case is much larger, thus enhancing fragmentation to occur towards the top portion of the chain.

The C_4D_9 fragments, in general, take longer time to eject. The momentum gained by the S in this case is weak so that only a small amount of energy is transferred to the chain. As a result, the recoil process occurs at the lower part of the chain which results in scission of the molecule to give a larger fragment. We do not observe the ejection of the lower part of the chain as its kinetic energy for ejection is insufficient to overcome the surface energy barrier.

The time distribution in Fig. 7 for $+55°$ angle of incidence does not reveal the same trend as that observed for $-35°$. In this case, it is commonly found that lateral motions of some fragmented species across the surface induce further fragmentation of neighbouring chains. An example of such mechanism is shown in Figs. 8(a) (e). The Ar atom first collides with one of the chains, causing it to fragment. Figs. 8(b) and (c) show that carbon atoms from the broken adsorbate move laterally to further collide with their neighbouring chains leading to the ejection of C_3D_7 and C_4D_9 fragments, Figs. 8(d) and (e). The fragments which are observed at short time scales of about 0.5 ps are thus mainly due to the direct impact of Ar atom to the hydrocarbon backbone of the chain.

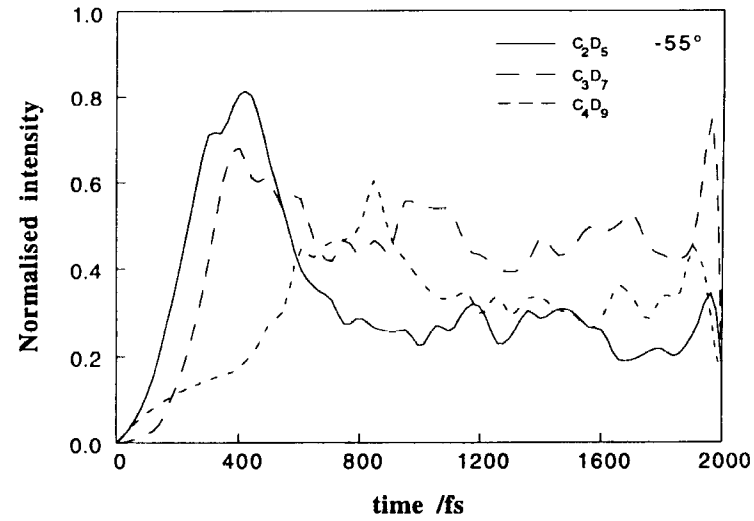

FIGURE 7 Time distribution for the ejection of the fragmented hydrocarbons with Ar at $+55°$ to the surface normal.

We also observed the ejection of intact thiol molecules (M, M–H where M is the complete alkanethiol molecule) for the $-35°$ impact although the intensity is rather low (16 counts for M ejection). For the $+55°$ angle, the signal for this species is very low (3 counts). It is thought that the direction of the Ar atom determines the momentum attained by the intact adsorbate atoms. We do not at this stage

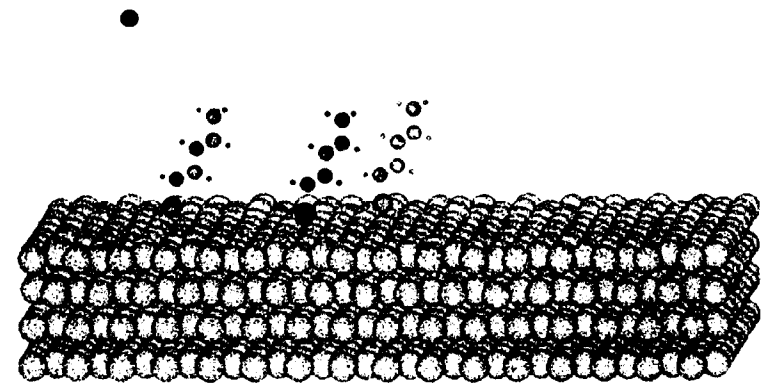

FIGURE 8(a)

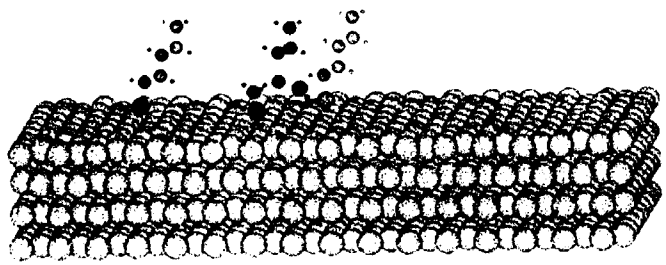

FIGURE 8(b)

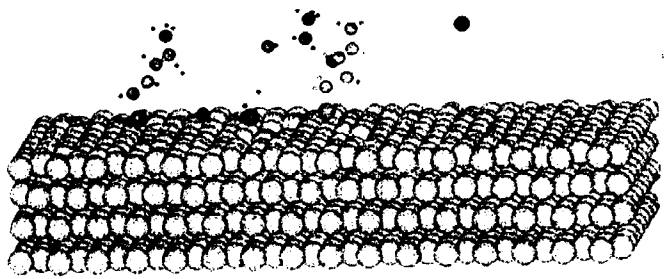

FIGURE 8(c)

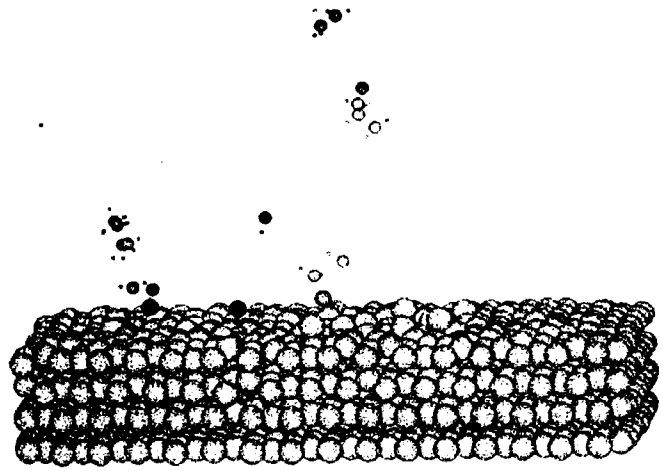

FIGURE 8(d)

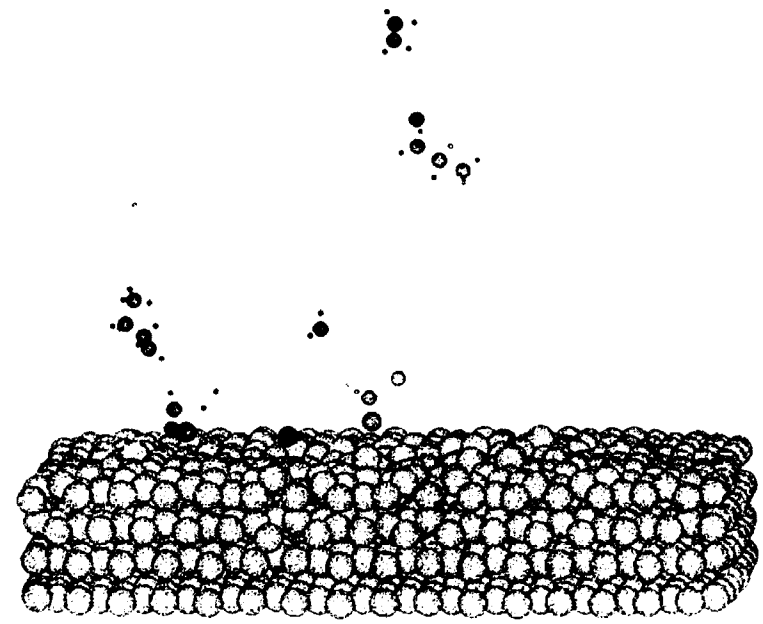

FIGURE 8(e)

FIGURE 8 Example of trajectory movie frames showing the formation of C_2D_5, C_3D_7 and C_4D_9 fragments. Only three chains relevant to the discussions are shown for clarity purpose. The light grey spheres represent Au atoms, and the red sphere represents Ar atom. The light red, dark grey and green spheres represent the whole thiol chains including S, C and H atoms. (a) 0 fs. The Ar atom is at +55° to the surface normal. (b) 6 fs. The Ar atom collides with the thiol chain (middle). (c) (d) 12–46 fs. Lateral collisions of the fragmented species with the neighbouring thiol chains. (e) 58 fs. Subsequent to these direct collisions the fragmented species eject at very short times. (See Color Plates XI–XV.)

however, intend to describe mechanistically how these species are ejected as this will be subjected to further investigation.

CONCLUSIONS

We have looked at the fragmentation behaviour of alkanethiol chains adsorbed on a Au(111) surface upon Ar atom bombardment at two different angles of incidence. We found high intensity of peaks corresponding to such hydrocarbon fragments as C_2D_5, C_3D_7, and C_4D_9 in both cases. A distribution of their times of ejection has been plotted for

the −35° impact angle (Fig. 5) which shows that C_2D_5 dominates at the shortest time scale whereas the C_4D_9 the longest. The C_3D_7 is the most abundant ejected species and we have suggested a mechanism for its ejection which also applies to the C_2D_5 and C_4D_9 formations. These, however, will depend upon the efficiency of the momentum transfer to the thiol chains. In other words, the larger the momentum is transferred to the thiols will lead to the formation of smaller hydrocarbon fragments. The time distribution observed for the +55° case (Fig. 7) is less significant as the fragmentation is largely due to the direct collision of the Ar atom with the adsorbates. This results in extensive fragmentation along the thiol chain at the selvedge region. The fragments from the broken chain move across the surface laterally to further collide with other thiol molecules leading to even more fragmentations.

The ability of MD simulations to monitor on an atomic level of what is happening in the adsorbate enables us to detail possible mechanisms involved in the bombardment-desorption process. We have also shown in this study that fragments having essentially identical masses can be resolved. Such a distinction may not be possible in experiments. We therefore believe that simulations of this kind using MD technique is able to provide valuable information by which experimental observables can be explained and predicted.

Acknowledgements

The support of the National Science Foundation through the Chemistry Division and the CRIF Program are gratefully acknowledged by BJG. The computer time was provided in part by the IBM SUR program. We appreciate helpful discussions with C.W. Yong.

References

[1] J.C. Vickerman, A. Brown and M. Reed, *Secondary Ion Mass Spectrometry* (Oxford, 1989).
[2] N. Winograd and B.J. Garrison, *Ion Spectroscopies for Surface Analysis* (Czanderna and Hercules, New York, 1991), pp. 45, 141.
[3] G.J. Leggett and J.C. Vickerman, *Intern. J. Mass Spectrom. Ion. Processes* **86**, 169 (1988).
[4] B.H. Sakakini, I.A. Ransley, C.F. Oduoza and J.C. Vickerman, *Surface Sci.* **271**, 227 (1992).
[5] R.S. Taylor and B.J. Garrison, *J. Am. Chem Soc.* **116**, 4465 (1994).
[6] A.M. Krallafa and J.H.R. Clarke, *J. Chem. Phys.* **91**, 6404 (1989).

[7] D.E. Harrison, N.S. Levy, J.P. Johnson and H.M. Effron, *J. Appl. Phys.* **39**, 3742 (1968).
[8] L.L. Lauderback, M.L. Ang and H.C. Murray, *J. Chem Phys.* **93**, 6041 (1990).
[9] A. Wucher and B.J. Garrison, *Surface Sci.* **260**, 257 (1992).
[10] R.S. Taylor, C.L. Brummel, N. Winograd, B.J. Garrison and J.C. Vickerman, *Chem. Phys. Lett.* **233**, 575 (1995).
[11] R.S. Taylor and B.J. Garrison, *Chem. Phys. Lett.* **230**, 495 (1994).
[12] R.S. Taylor and B.J. Garrison, *Langmuir* **11**, 1220 (1995).
[13] G. Gillen, S. Wight, J. Bennett and M.J. Tarlov, *Appl. Phys. Lett.* **65**, 534 (1994).
[14] C.E.D. Chidsey, G.Y. Liu, P. Rowntree and G.J. Scoles, *J. Chem. Phys.* **91**, 4421 (1989).
[15] L. Strong and G.M. Whitesides, *Langmuir* **4**, 546 (1988).
[16] L.H. Dubois, B.R. Zegarski and R.G. Nuzzo, *J. Chem. Phys.* **98**, 678 (1993).
[17] J. Hautman and M.L. Klein, *J. Chem. Phys.* **93**, 7483 (1990).
[18] M.P. Allen and D.J. Tildesley, *Computer Simulation in Liquids* (Oxford, 1987).
[19] H. Sellers, A. Ulman, Y. Shnidman and J.E. Eilers, *J. Am. Chem. Soc.* **115**, 9389 (1993).
[20] J.B. Gibson, A.N. Goland, M. Milgram and G.H. Vineyard, *Phys. Rev.* **120**(4), 1229 (1960).
[21] B.J. Garrison, *Chem. Soc. Rev.* **21**, 155 (1992).
[22] The correction to the screening factor in the Moliere equation (5) of D.J.O'Connor and R.J. MacDonald, *Radiation Effects* **34**, 247 (1977). The complete Moliere equation is also given herein.
[23] M.S. Stave, D.E. Sander, T.J. Raeker and A.E. DePristo, *J. Chem. Phys.* **93**, 4413 (1990).
[24] T.J. Raeker and A.E. DePristo, *Int. Rev. Phys. Chem.* **10**, 1 (1991).
[25] S.W. Rosencrance, J.S. Burnham, D.E. Sanders, C. He, B.J. Garrison, N. Winograd, A. Postawa and A.E. DePristo, *Phys. Rev. B: Condensed Matter* **52**, 6006 (1995).
[26] D.W. Brenner, *Phys. Rev. B* **42**, 9458 (1990).
[27] D.W. Brenner, J.A. Harrison, C.T. White and R.J. Colton, *Thin Solid Films* **206**, 220 (1991).
[28] L.A. Girifalco and V.G. Weizer, *Phys. Rev.* **114**, 687 (1959).